Towards the biomimetic design of hollow fiber membrane bioreactors for bioartificial organs and tissue engineering: a micro-computed tomography (μCT) approach

Giuseppe Falvo D'Urso Labate[a,#], Thomas De Schryver[b,§], Francesco Baino[c], Charlotte Debbaut[d], Gionata Fragomeni[e], Chiara Vitale-Brovarone[c], Luc Van Hoorebeke[b], Patrick Segers[d], Matthieu Boone[b], Gerardo Catapano[a,*]

[a]Department of Mechanical, Energy and Management Engineering, University of Calabria, Via Pietro Bucci, 87036 Rende (CS), Italy. E-mails: gvufdl@yahoo.it (GFDL); gerardo.catapano@unical.it (GC)

[b]UGCT-Rad. Phys., Dept. of Physics and Astronomy, Ghent University, Gent, Belgium. E-mails: thomas.deschryver@tescan.com (TDS); luc.vanhoorebeke@ugent.be (LVH); Matthieu.Boone@UGent.be (MB)

[c]Department of Applied Science and Technology, Politecnico di Torino, C.so Duca degli Abruzzi 24, 10129 Torino, Italy. E-mails: francesco.baino@polito.it (FB); chiara.vitale@polito.it (CVB)

[d]IBiTech - Biommeda, Department of Electronics and Information Systems, Ghent University, Campus UZ, Blok B – entrance 36, Corneel Heymanslaan 10, B-9000 Gent, Belgium. E-mail: charlotte.debbaut@ugent.be (CD); patrick.segers@ugent.be (PS)

[e]Department of Medical and Surgical Sciences, Magna Graecia University, Catanzaro, Italy. E-mail: fragomeni@unicz.it (GF).

*Corresponding author:
phone: +390984496666
e-mail address: gerardo.catapano@unical.it

Present addresses:
[#]Cellex srl, Piazzale delle Belle Arti 2, 00196 Roma, Italy
[§]TESCAN XRE, Bollebergen 2B box 1, 9052 Gent, Belgium

Abstract

Hollow fiber membrane bioreactors (HFMBs) with cells cultured in the extracapillary space (ECS) have been proposed for bioartificial organs, to assist patients with failing organs, or to produce *in vitro* engineered biological substitutes of tissues and organs. They have not gained clinical acceptance yet. One factor limiting therapeutic application is the irregular membrane distribution in the HFMB shell, often considered a typical feature of clinical-scale HFMBs. Such distribution does not permit good control of shell spaces, prevents from offering cells a template structure mimicking the tissue-specific extracellular matrix (ECM) and an adequate supply of oxygen and nutrients, and limits control over cell migration, organization, and differentiation in the ECS.

In this study, micro-computed tomography and image analysis techniques were used to characterize the space distribution in the shell of HFMBs varying for membrane packing density and bundling technique, and to investigate whether and how it is possible to manufacture HFMBs in which the distribution of intermembrane spaces in the ECS is uniform and biomimetic.

Results suggest that the arrangement in HFMBs of hollow fiber membranes bundled in rolled cross-woven mats at high packing density permits to obtain a uniform shell-side membrane distribution with pore size distribution favoring cells migration around the membranes, and mimicking the ECM structure of bone tissue.

1. Introduction

Already about 50 years ago Knazek et al showed for the first time that fibroblasts and choriocarcinoma cells could be effectively cultured at *quasi-in vivo* cell density outside and around parallel hollow fiber membranes arranged in a bioreactor in the shell-and-tube configuration [1]. Since then, hollow fiber membrane bioreactors (HFMBs), mainly operated in the tube-feed and closed-shell mode, have been proposed for the culture of a large variety of mammalian cells for biotechnological and therapeutic purposes [2,3]. The main reason is that feeding oxygen (O_2) and nutrients-rich medium into the membrane lumina (i.e. the intracapillary space, ICS) permits a delocalized and distributed supply of dissolved O_2 and nutrients to the cells in the bioreactor shell (i.e. the extracapillary space, ECS) and an effective removal of metabolic wastes similar to that occurring *in vivo*. The use of hollow fiber membranes reduces the solute diffusion pathlength and transport resistance to/from the cells, prevents possible metabolic inhibitors from accumulating, and protects cells from undesirable mechanical stresses. Over the years, membranes and design criteria have been developed for HFMBs to effect pure diffusive [4-6] or convection-enhanced [7-10] transport of dissolved oxygen, nutrients and other biochemicals from the medium to the cells (and vice versa), or to timely switch from one transport mechanism to the other during culture to match nutrients supply to the changing cell metabolic requirements. HFMBs may also be easily scaled-up, enable non-conventional bioreactor designs, and are flexible in operation. In medicine, HFMBs have been proposed as the core of bioartificial organs [11], to temporarily assist patients with failing organs till organ transplantation or recovery, or to produce *in vitro* engineered biological substitutes of tissues and organs at the clinical scale [3]. In such applications, the hollow fiber membranes provide large surfaces to scaffold therapeutically effective amounts of cells in small bioreactor volumes, thus minimizing the bioreactor priming volume. The membranes may act as immune-isolation barriers that protect allogeneic, xenogeneic and line cells against rejection of the host without (or with minimal) need for immune suppressive drug treatment [12]. HFMBs in the shell-and-tube configuration bear also structural and functional resemblance to some human tissues, such

as liver and bone. In fact, cells seeded in the ECS of HFMBs may organize around the hollow fiber membranes similar to how cells organize *in vivo* around the sinusoids in the liver and the Haversian canals in the bone. Similar to such natural vessels, the membranes effectively supply cells with nourishment and remove metabolic wastes. Nonetheless, to the best of our knowledge, therapeutic treatments based on HFMBs have not gained clinical acceptance yet. In spite of the various and innovative HFMB concepts that have been proposed to culture primary or line hepatic cells to assist hepatopathic patients (i.e. in bioartificial livers, BALs), just a few have reached clinical testing and none has shown clear therapeutic efficacy yet. Choice of the cell types, suboptimal cell distribution in the ECS, unphysiological presentation of dissolved oxygen, nutrients and biochemical cues to cells and consequent poor cell (re)differentiation, and the ineffective return to patient circulation of liver-specific species synthetized by the cells apparently still limit their therapeutic efficacy [11,13]. In the *in vitro* engineering of bone tissue, HFMBs in the shell-and-tube configuration operated in convection-enhanced closed-shell mode have been shown to promote stem cell differentiation to the osteoblast phenotype and to permit culture at close to *in vivo* cell concentrations [14]. The difficult control of cell distribution in the ECS and the limited availability of highly permeable bioresorbable membranes still limit their potential in the preparation of biological substitutes of bone tissue. This suggests that there is a great need to improve on the design of HFMBs, in particular to control cells distribution, organization, and growth in the ECS, to make them therapeutically effective and gain clinical acceptance of HFMB-based treatments. Over the years, evidences have accumulated suggesting that a biomimetic tissue engineering approach to HFMB design could lead to the development of therapeutically effective bioreactors and could help engineer *in vitro* biological constructs similar to natural tissue [15-17]. Consistent with the biomimetic tissue engineering approach to develop fully functional liver and bone tissue, considerable research efforts have been and are being devoted to optimizing (i) the choice of the cell types, (ii) the selection and timely administration of biochemical and mechanical cues to guide cell organization, differentiation and the expression of such functions as in the natural tissue, (iii) the choice of membrane transport and

separation properties, and (iv) the HFMB design criteria to ensure dissolved oxygen and nutrients supply matching the time-changing metabolic requirements of a clinically significant mass of cells as tissue matures. Reviewing progresses in these fields is beyond the scope of this paper and references may be found in literature [e.g., 18,19].

In the biomimetic engineering of tissues, an important role is considered to be played by the properties of the scaffold that replaces the natural tissue-specific extracellular matrix (ECM) [20]. There is general agreement that the scaffold microarchitecture should mimic the natural ECM, and it should provide cells with similar immobilized and soluble biochemical signals [21]. This way only the scaffold is expected to foster the 3D organization of multiple tissue-specific cell types as in the natural tissue. There is also general agreement on the fact that the scaffold should exhibit a bimodal pore size distribution to permit cell migration, attachment, and uniform colonization through larger pores, and the supply of dissolved oxygen and nutrients through smaller pores to ensure survival of a large and dense clinical-scale cell mass [22]. Different from this, the HFMBs for engineering *in vitro* liver and bone tissue have been, and still are, typically designed mainly to feature shell volumes capable of hosting a clinically relevant cell mass, and are equipped with membranes which should mainly ensure immune protection of the cellular graft. The basic theoretical assumption in their design is that membranes are uniformly distributed in the shell of HFMBs, and provide enough space for unhindered cell migration into the membrane bundle as well as uniform provision of nourishment and biochemical cues for cells to survive and organize as in natural tissue. The HFMB geometry and operation is typically optimized with flow and mass transport models assuming that (i) membranes are arranged parallel to one another in a regular hexagonal pattern, (ii) each membrane is surrounded by a uniform annulus of ECS at most two cell-layers thick (i.e. generally thinner than about 50 μm) when solutes are transported by pure diffusion to (or away from) cells, and (iii) cells viability is preserved anyway [6]. Different from this, experimental studies on modules for hemodialysis [23-26] and technical applications [27,28] have shown that the hollow fiber membrane distribution in the module shell is not generally uniform.

Non-uniform hollow fiber spacing in the shell is reported to cause flow maldistribution and decrease the efficiency of solute transfer across the membranes. Insertion of spacer yarns and baffles in the ECS to some extent enhances solute lateral mixing and minimizes the detrimental effects on transport of membrane irregular distribution [22,27,29,30]. Such solutions are impractical for HFMBs in which cells are cultured in the ECS. Doubts also exist on the possibility that cells seeded in the HFMB shell might freely and uniformly migrate around membranes in the bundle when the intermembrane distance is less than about 100 μm. An uneven 3D membrane distribution in the HFMB shell may be expected to hinder cell migration in the shell regions where membranes are densely packed, to cause an uneven cell distribution, to hinder control of cell differentiation and a uniform supply of dissolved oxygen and nutrients matching cell metabolic requirements, and even to cause cell death. The irregular membrane distribution in the ECS is often accepted as a typical feature of clinical-scale HFMBs which structurally limits their use for therapeutic applications [6]. To the best of our knowledge, the actual distribution of hollow fiber membranes in the shell of HFMBs proposed for engineering natural tissues *in vitro* has not yet been directly characterized in quantitative terms, nor have fabrication techniques been investigated to obtain uniform intermembrane spaces of controlled size in the ECS, nor has it been characterized to which extent the architecture of spaces in the ECS mimics the ECM architecture of natural tissue.

In this study, microcomputed tomography (μCT) and image analysis techniques were used to characterize the distribution of spaces in the shell of HFMBs varying for membrane packing density and bundling technique. The aim was to investigate whether and how it is possible to manufacture HFMBs in which a uniform and biomimetic distribution of intermembrane spaces in the ECS may be obtained. To this purpose, the intermembrane space distribution in the shell of HFMBs was characterized in terms of architectural parameters influencing cell migration, attachment and osteointegration and it was compared to natural equine femur tissue and a commercial hydroxyapatite scaffold used in the clinics as synthetic bone substitute.

2. Materials and Methods

2.1   Membrane modules

In-house built hollow fiber membrane bioreactors used for this study were equipped with microporous polypropylene hollow fiber membranes (280 μm inner diameter, 50 μm wall thickness, 0.1 μm maximal micropore size) provided either in loose bundles (LB) or bundled in rolled cross-wound (CW) membrane mats (Figure 1). In the CW mats used for this investigation, membranes were orderly
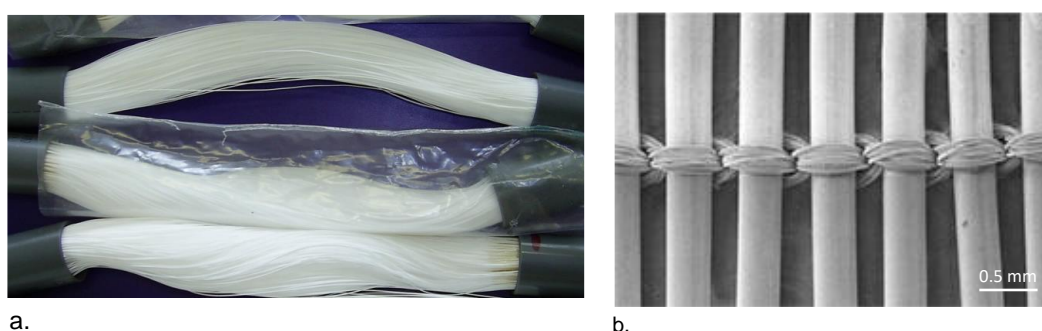

a.

b.

Figure 1. Membrane bundling techniques used for this study: a) membranes arranged in loose bundle, LB; b) membranes arranged in cross-woven mats, CW. Figures reproduced with permission from the Separation and Purification Sciences Division (SPSD) of 3M Wuppertal (Germany).

held at a distance of about 300 μm from one another by knitting with polyester threads at approximately 90 degrees with respect to the bioreactor axis. An operator unaware of the study assembled the laboratory-scale bioreactors in the shell-and-tube configuration by fitting either membrane bundle in a cylindrical housing, by potting the bioreactor ends with glue, and by cutting the excess membrane length with a sharp blade. The intracapillary and extracapillary spaces of the HFMB were then equipped with conical and cylindrical inlet and outlet ports, respectively, as schematically shown in Figure 2. High packing density (HD) modules were manufactured that contained approximately 400 membranes/cm^2 cross-sectional area, and low packing density (LD) modules with approximately 20 membrane/cm^2 cross-sectional area. Membranes and membrane modules were kindly provided on specification for this investigation by the Separation and Purification Sciences Division (SPSD) of 3M (former Membrana GmbH), Wuppertal, Germany.

2.2 Characterization of the HFMB shell space

The architectural features of the spaces outside and among the HF membranes constituting the ECS (hereinafter referred to also as "pores") in the HFMB shell were characterized by micro-computed tomography and image analysis, as described below. In the analysis the contribution of membrane lumina (i.e. the ICS) to the shell fractional space volume was excluded. Pore size and the axial uniformity of the pore distribution was qualitatively characterized by analyzing binarized 2D images of bioreactor cross-sections at the bioreactor half-length and at one end. The uniformity of the shell porosity (i.e. the space fractional volume) in the cross-section was characterized in quantitative terms by evaluating the shell porosity in four quadrants of a central and a peripheral concentric zone, each half shell radius wide, at the bioreactor half length. The microarchitecture of the intermembrane space in the ECS was characterized in terms of its porosity ε, mean pore size, pore interconnectivity I_p, specific surface area a_v, degree of anisotropy DA, and connectivity density β, as described below in detail. Its biomimicry was assessed by comparison to natural equine femur trabecular bone tissue (EFT) (tradename Osteoplant®, OSP01) (kindly provided by Bioteck, Arcugnano (VI), Italy) and to a narrow pore hydroxyapatite scaffold (NPHA) commercially available as synthetic bone substitute (tradename EngiPore® - PFS015005-23-00) (kindly provided by Finceramica, Faenza, Italy). The characterization methods and the features of both benchmark materials were already reported in a previous investigation [31]. For this reason, their description may resemble that reported in [31], occasionally *verbatim*.

2.3 Image acquisition

High-resolution microtomographic images of shell-side membrane distribution were acquired in two HFMBs of each type and were analyzed as schematically shown in Figure 2. 2D cross-sectional images were acquired with a Bruker SkyScan 1174 (Bruker Corporation, Billerica, MA, USA) and the High-Energy CT system Optimized for Research (HECTOR) micro-computed tomography (μCT) scanner [32]. The latter was specifically developed for research by the Ghent University

8

Centre for X-ray Tomography in collaboration with X-Ray Engineering (XRE bvba, Ghent, Belgium). The two μCT systems were operated at 50 kV, 800 μA and 140 kV, 71 μA, respectively.
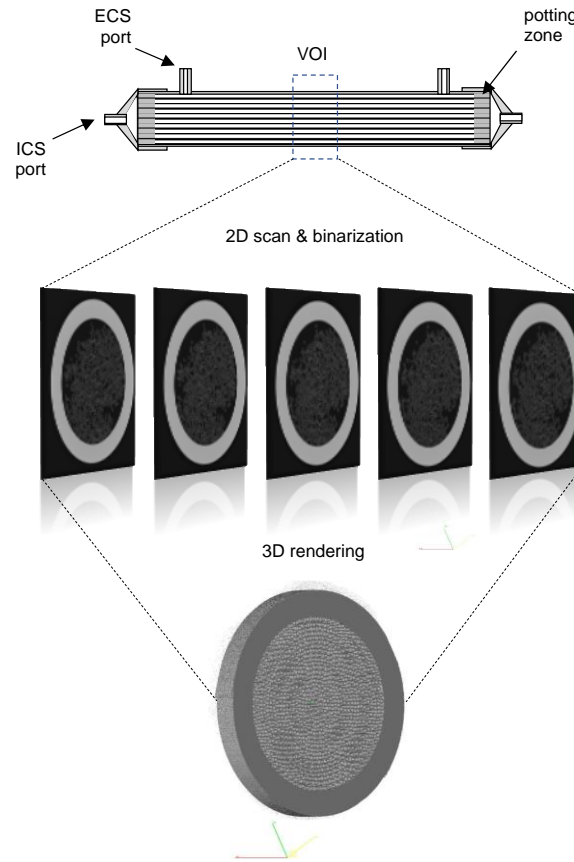

Figure 2. 3D bioreactor rendering. Scheme of the procedure to render in 3D the membranes (and spaces) distribution in the shell of hollow fiber membrane bioreactors in the shell-and-tube configuration starting from raw 2D images of bioreactor cross-sections acquired by micro-computed tomography: ECS – extracapillary space; ICS – intracapillary space; VOI – volume of interest.

Scans and images of bioreactor cross-sections were acquired at the bioreactor half-length and at one end in a cylindrical volume of interest (VOI) 10 mm long with a diameter equal to the bioreactor shell. The isotropic voxel size was typically between 9^3 μm^3 and 10^3 μm^3. 2D images of shell cross-sectional layers were acquired, binarized and reconstructed from raw μCT data by means of the standard filtered backprojection algorithm [33] with the software Octopus Reconstruction version 8.8.6.1 1 (Tescan Orsay Holding a.s., Brno–Kohoutovice, Czech Republic) obtaining 16-bit grey-value images. The data thus obtained were imported in the software Mimics® (Materialise, Leuven,

9

Belgium) and rescaled in the 0-65,536 range. The resulting grey-level histogram exhibited three peaks, a fully resolved peak for the ECS and two partly overlapping peaks for the fibers and the plastic housing. The peaks were approximated with a normal distribution and voxels were considered which had a grey-value falling in the interval between the mean value (μ) plus or minus two times the standard deviation (σ) of the given peak (i.e. $\mu + 2 \cdot \sigma$). The solid material voxels were separated from the void voxels based on their grey-scale value (i.e. were segmented) with a lower 6,000 grey threshold value and an upper 18,000 grey threshold value in the fiber domain, and a lower 14,620 grey threshold value and an upper 29,709 grey threshold value in the housing domain. The software Mimics® was used to isolate the overlapping peaks and to render the binary 3D representation of the membrane distribution and of the outer housing in each VOI starting from the 2D images. Background information on these methods can be found in [22, 34-36].

2.4 Image analysis

The pore architecture in each VOI was characterized with ImageJ (NIH, Bethesda, MA, USA) in terms of parameters enabling cell migration, scaffolding and nourishment in the bioreactor shell, in analogy to those used for characterizing porous scaffolds for tissue engineering and natural extracellular matrix and to that described in [31]. Prior to estimating the architectural parameters, the membrane lumina were filled automatically with a region-filling algorithm [37]. Briefly:

porosity, ε - the shell porosity was defined as the fractional VOI volume occupied by the shell spaces, and was estimated as the shell space-to-total voxel ratio in each VOI. The ICS was excluded throughout;

mean pore size – any group of void voxels in the ECS surrounded by solid voxels was considered as a pore. The pore size distribution was estimated according to a model-independent two-step procedure. Firstly, the medial axis of all void structures was identified (i.e., skeletonization). Secondly, a "sphere-fitting" measurement was performed for all the voxels lying along each axis. The local size associated to a point on each axis was defined as the mean diameter of the spheres fulfilling the following two conditions: 1. the sphere encloses the point, but the point is not

necessarily the center of the sphere; 2. the sphere is entirely enclosed in the void structure, but it is

entirely bounded within the solid surfaces [31]. The local sizes of the obtained void structures were

distributed in classes and the fractional number of local sizes falling in each class was estimated.

The size range of each class was set equal to twice the size of the voxel of the considered micro-

computed tomography scan. Finally, the mean pore size was estimated as the mean value over all

the classes;

pore interconnectivity, I_p – the pore interconnectivity was defined as the fraction of the void volume

in the VOI that maintains connections with air surrounding the membrane assembly, and it was

estimated as follows [38]:

$$I_p = Po.O/\varepsilon \quad . \tag{1}$$

Po.O is the open pore-to-VOI volume ratio, and ε is the shell porosity. *Po.O* was estimated as the

complement to one of the closed porosity. The closed porosity is the fractional volume of closed

pores in the VOI. Herein, a closed pore is defined as a connected assembly of void voxels

completely surrounded by solid voxels in 3D;

specific surface area, a_v - the specific surface area provides a measurement of the solid surface area

available for cell attachment per unit scaffold volume, and was estimated as follows:

$$a_v = BS/TV \tag{2}$$

where: *BS* is the membrane surface measured based on the faceted surface of the marching cubes

volume model [39] and *TV* is the total number of voxels in the VOI;

degree of anisotropy, DA - the degree of anisotropy is a measure of the preferential alignment of

solid surfaces (e.g., the HF membranes) in the bioreactor shell along given directions, and was

estimated according to the mean intercept length (MIL) analysis [35]. The MIL was obtained by

drawing a line through a 3D imaged volume containing binarized objects at any 3D orientation, and

by dividing the length of the test line through the VOI by the number of times that the line passes

through or intercepts part of the solid material in any direction. The MIL distribution was computed

by drawing parallel test lines in varying directions on the 3D image. The MIL ellipsoid was

computed by least-square fitting the directional MIL to a directed ellipsoid. Eventually, the *DA* was estimated as the complement to one of the minimal-to-maximal radius ratio of the MIL ellipsoid. A detailed description of the MIL analysis may be found in [35]. Values of *DA* close to 0 indicate that the intermembrane space distribution in the HFMB shell is isotropic. Values of *DA* close to 1 indicate an anisotropic distribution;

Euler connectivity, Eu.Conn - Eu.Conn characterizes the redundancy of trabecular connections in the VOI and it provides a measure of the number of connections that must be severed to break down the intermembrane space in two separate parts [35]. It is derived from the Euler characteristic, *EC*, which accounts for the number of cavities surrounded by solid material. Details on how *EC* was estimated from the binarized images can be found in [40]. The connectivity of each VOI was estimated as follows:

$$Eu.conn = 1 - EC \qquad . \qquad (3)$$

connectivity density, β - To characterize the intermembrane space in the VOI independent of its size, the connectivity was normalized with respect to the VOI volume, *TV*, and was expressed as the *connectivity density, β*, as follows [35]:

$$\beta = Eu.Conn/TV \qquad . \qquad (4)$$

The parameter values for each investigated HFMB type were estimated from the images of the cross-sections of both prototypes that were amenable to digitalization with little bias. They are generally reported as mean ± standard deviation. The Kolmogorov-Smirnov test was used to verify that the distribution of such data is Gaussian [41].

3. Results and Discussion

Preparing HFMBs with hollow fiber membranes in loose bundles is the standard procedure. The technique for weaving hollow fiber membranes in mats with the aid of polyester threads has been developed in the early '90s [42]. The possibility of keeping the membranes orderly spaced and angled in the mat was effectively exploited in the preparation of blood-outside oxygenators, where

blood flows outside and among the membranes in channels of well-defined geometry [43]. In spite of the advantages and flexibility that they offer in the preparation of modules, membrane mats are seldom used to prepare HFMBs for engineering tissues or organs. Aim of this study was to systematically investigate their possible use for such purpose.

The 2D images of bioreactor cross-sections obtained by μCT showed that the actual membrane packing density was within 15% of its design value. The HFMB shell space (hence its porosity) consisted of spaces outside and among the hollow fiber membranes (i.e. the intermembrane space), and spaces between the outer periphery of the membrane bundle (which was sometimes highly irregular) and the housing inner surface (i.e. the peripheral space), as shown in Figure 3. The fractional extent and spatial uniformity of these spaces changed with the distance from the shell ports, and depended on the distance among neighboring membranes and on the position (e.g. coaxial or eccentric) and width of the membrane bundle in the housing. It is worthwhile noting that in most transport models of HFMBs the peripheral space is generally neglected, so are the spaces in between the annuli surrounding neighboring membranes according to the Krogh model [e.g. 5,6,8,10]. In analogy to the microarchitectural characterization of porous scaffolds for tissue engineering, in this study the radial uniformity of shell space distribution was assessed with respect
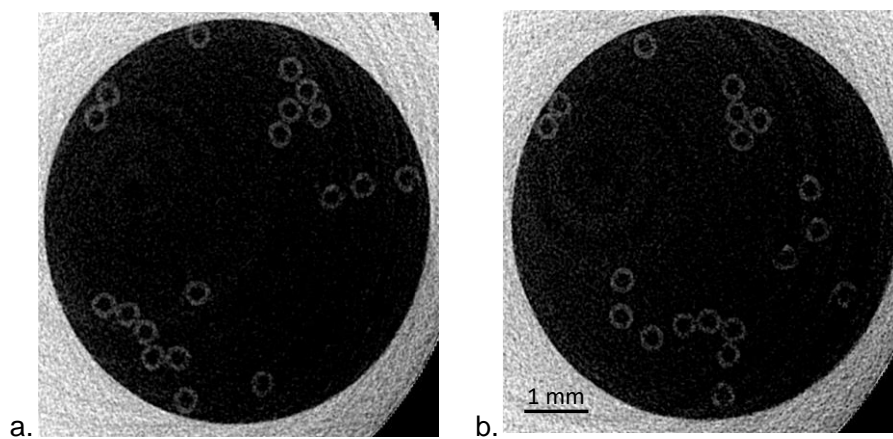

Figure 3. Exemplary 2D images acquired by μCT of cross-sections of HFMBs equipped with low packing density of membranes provided in loose bundles (LD-LB HFMB). Images acquired at one end (a) or at the half-length (b) of the bioreactor.

to the intermembrane space because this space has the greatest influence on cell migration, scaffolding and nourishment supply deep into the membrane bundle. HFMBs with high and low membrane packing densities were investigated because, for a given theoretical intermembrane distance, the bundle width depends on the number and geometry of the hollow fiber membranes in the bioreactor cross-section.

3.1 Uniformity of space distribution

As an effect of membrane potting, at the end of all HFMBs, and in proximity of the shell ports, the hollow fiber membranes clustered more densely around the bioreactor axis and a circular peripheral space formed near the housing that was devoid of membranes. The membranes were gradually distributed over larger bioreactor cross-sectional areas towards the bioreactor half-length. This HFMB feature permits to distribute the cell suspension seeded through the shell ports uniformly around the membrane bundle periphery and along the bioreactor length, and then radially into it. Thickness, shape and axial length of the circular peripheral space depended on membrane packing density and on whether the membranes were arranged in the housing as loose bundle or rolled cross-woven mat.

In the HFMBs equipped with membranes provided in loose bundle at low packing density (i.e. LD-LB HFMBs), the hollow fiber membranes distributed in very non-uniform fashion over the bioreactor cross-sectional area anywhere in the bioreactor, as shown in Figure 3. Even at the bioreactor half length, the membranes were sparsely distributed and, in some zones, they formed small clusters distant from one another by as much as 2 mm. In other zones, there were just a few, or single, membranes many millimeters distant from one another and from the clustered membranes.

Figures 4a,c show that in HD-LB HFMBs the higher average membrane packing density favored a more uniform distribution of the shell spaces. Close to the periphery of the bioreactor end, the circular peripheral space devoid of membranes was rather irregular and thick (from about 0.7 mm to a few millimeters). At the bioreactor half-length, some membrane-free spaces were still present in a

few zones. The membrane packing density was irregular and varied by up to a factor 2.5 in different quadrants of the cross-section periphery (data not shown). In some zones, membranes were tightly packed occasionally causing the deformation of the membrane wall. In other zones, membranes
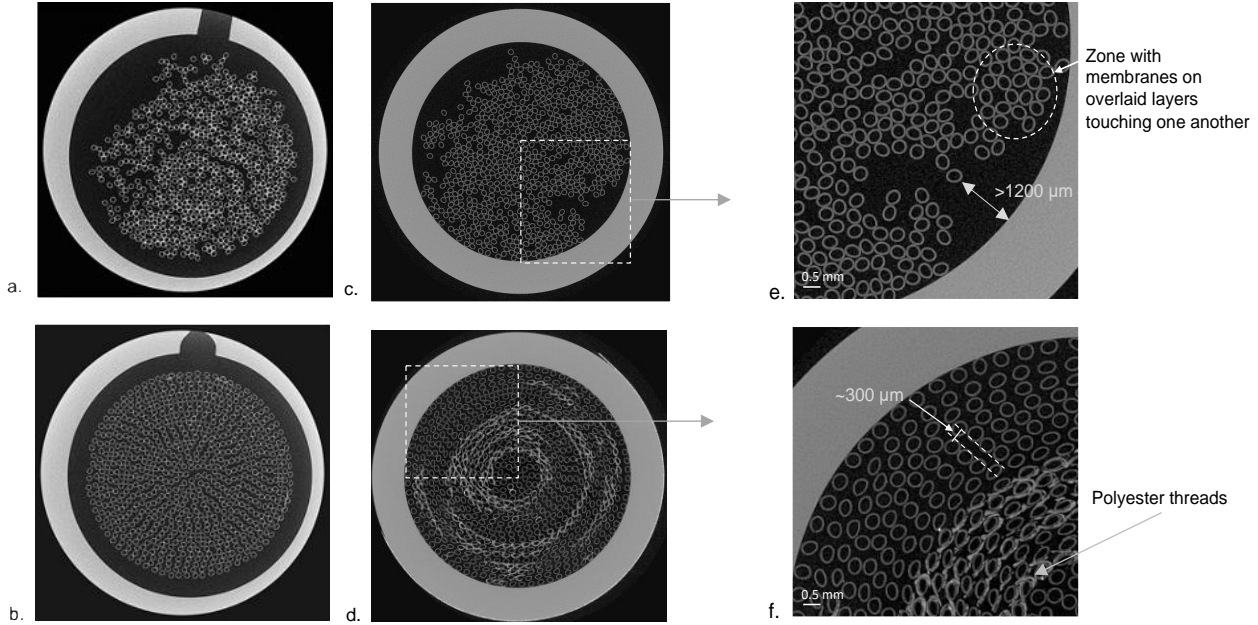

Figure 4. Exemplary 2D images acquired by µCT of HFMB cross-sections. Images acquired at one end (a,b) or at the half-length (c-f) of HFMBs equipped with high packing density of membranes in various bundle types: a,c,e) loose bundles (HD-LB); b,d,f) cross-woven mats (HD-CW). Images in Figures 4e,f are magnifications of the images reported in Figures 4c,d, respectively.

were totally absent forming void sectors a few millimeters large, as shown in Figure 4d. Close to the bioreactor axis, membranes were more regularly and tightly distributed. Such distribution yielded a mean intermembrane distance of about 660 µm. Figures 4b,d,f show that in HD-CW HFMBs the use of densely packed cross-woven membrane mats generally resulted in a uniform distribution of both peripheral and intermembrane spaces. At the HFMB end, the circular space at the shell periphery devoid of membranes was more regular and thinner than in HD-LB HFMBs. At the bioreactor half-length the peripheral space thickness was not significantly greater than the distance among membranes in overlaid layers. The fractional cross-sectional area of the intermembrane pores was rather uniform from the bioreactor end to half-length. Figure 4f shows that the membranes were consistently spaced apart defining radial channels from the bundle

15

periphery to the center about 300 μm large, and circumferential channels among membranes in overlaid layers a few tens of microns large.
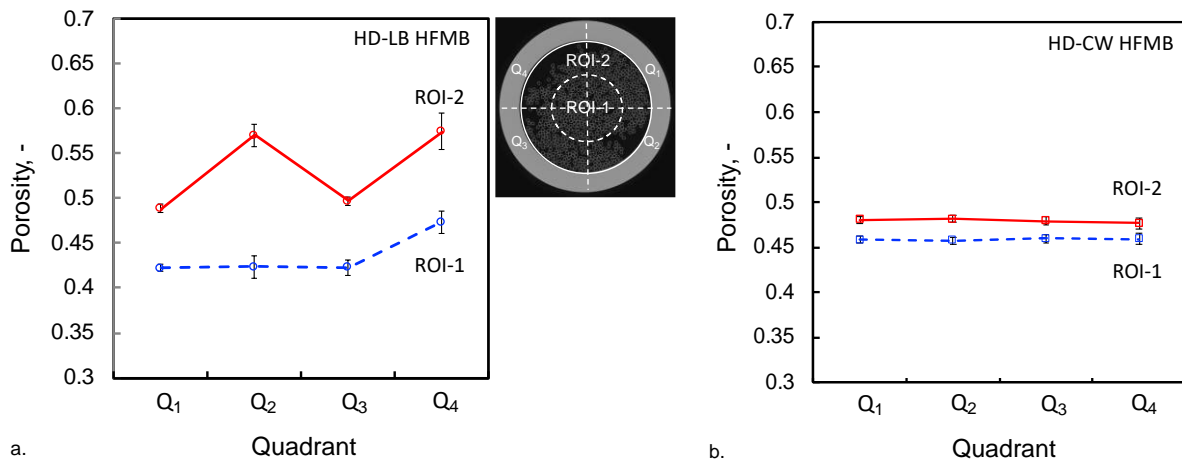

Figure 5. *Mean intermembrane porosity in various quadrants of bioreactor shell cross-sections (Region of interest, ROI, 1&2). Images acquired at the half-length of HFMBs prepared with membranes differently bundled and packed at high membrane density: a) loose bundle, HD-LB; b) cross-wound mat, HD-CW. ROI-1 (dashed lines) and ROI-2 (solid lines) identify a central and a peripheral zone in the HFMB cross-section, respectively, as shown in the inset of the left panel. In the same inset the quadrant (Q_i) position is shown.*

Figure 5 shows that the quantitative characterization of the shell porosity in various zones of the bioreactor cross-section at half-length was consistent with the membrane distribution in the HFMB shell shown in Figure 4. In the cross-section of HD-LB HDMBs, the shell porosity was erratic and non-uniform in zones of the periphery (i.e., ROI2), varying by as much as 17.5% (Figure 5a), with membrane densities in some zones of ROI2 up to 3.1 times higher than in the bioreactor center (i.e. ROI1) (data not shown). At the bioreactor center, the shell porosity was generally more uniform except in those quadrants in which the membrane-free gaps in the periphery propagated to the bioreactor axis (e.g. in Figure 4a). Figure 5b shows that the shell porosity in HD-CW HFMBs was in the range of many ceramic and metal scaffolds proposed for bone regeneration [22], and was rather uniform over the entire bioreactor cross-section with minimal (i.e. about 5%) variation between the periphery and the center. The analysis of the μCT images yielded the parameters characterizing the space microarchitecture of the HD-HFMBs reported in Table 1. They are consistent with those shown in Figures 4-5. Different from what is generally accepted as an intrinsic

limit of HFMBs, they show that HFMBs equipped with membranes densely bundled in CW mats may be manufactured in such a way that they exhibit uniform and highly interconnected shell spaces with well controlled size distribution. Such spaces meet the criteria for porous TE scaffolds to ensure uniform cell migration throughout the membrane bundle, uniform nutrient supply to cells anywhere in the bundle, and to offer a large specific surface area for cell attachment comparable to porous scaffolds for tissue regeneration. It is worth noting that in HD-CW HFMBs pores of different size along the bioreactor radius, circumference, and length may be realized by varying the number of membranes knitted together per unit mat length, and the thickness of the spacer interposed in between the rolled mat layers.

	HD-LB HFMB	HD-CW HFMB	Natural EFT[*]	Synthetic NPHA scaffold[*]
Porosity, %	48.4±0.06	45.8±0.01	65.4±0.38	73.0±0.35
Pore interconnectivity, %	81	99	100	100
Mean pore size, mm	661±314	303±4	433±194	416±211
Specific surface area, mm^{-1}	4.03±0.35	5.71±0.05	8.05±0.67	9.38±0.09
Degree of anisotropy, -	0.90	0.97	0.72	0.08
Connectivity density, mm^{-3}	5.93±0.26	8.47±0.04	18.3±10.7	96.5±3.43

Table 1. Architectural parameters of the space distribution in HFMBs varying for membrane packing density and bundling technique: HD-LB HFMB - HFMBs prepared with loose bundles of membranes at high packing density; HD-CW HFMB - HFMBs prepared with rolled cross-woven mats of membranes at high packing density; Natural EFT – natural trabecular bone of equine femur; Scaffold NPHA – commercial narrow pore hydroxyapatite bone substitute. [*] data from [31].

3.2 Biomimicry of space distribution

The biomimicry of the space architecture in the HFMB shell was assessed at the bioreactor half-length. In fact, as noted above, close to the shell ports of HFMBs the membrane bundle is willingly set at a distance from the housing to facilitate uniform cell delivery along the bioreactor length. To evaluate the extent to which the intermembrane space architecture in the ECS of HFMBs mimics natural bone tissue, its main features were compared to equine femur trabecular tissue and a synthetic commercial bone substitute characterized according to the same methods as in a previous
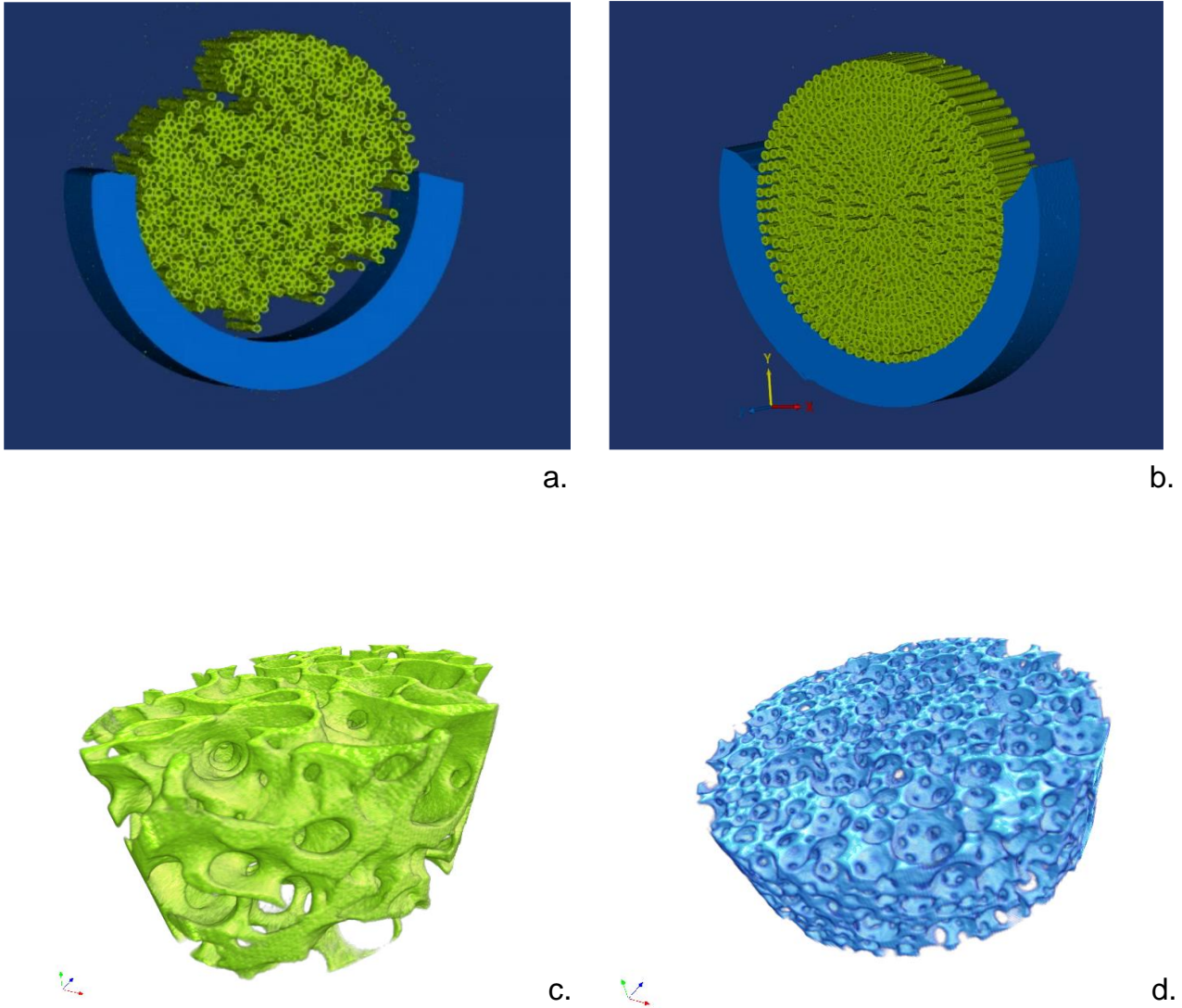
a.

b.

c.

d.

Figure 6. 3D rendering of micro-computed tomographic images of various scaffolding structures suitable for bone tissue engineering: a) HD-LB HFMB; b) HD-CW HFMB; c) trabecular bone of natural equine femur, EFT [31]; d) commercial narrow-pore hydroxyapatite bone substitute, NPHA [31]. Figures 5c,d reproduced with permission from SAGE Publishing Inc..

study [31]. Figure 6 shows that the intermembrane pores in the ECS of HFMBs featured an elongated morphology, mainly parallel to the bioreactor axis, and were highly interconnected along the bioreactor radius. Such space architecture may seem different from the natural trabecular bone tissue and the synthetic bone substitute in which pores form as spaces among the convoluted flat bony trabeculae or the struts of the ceramic material. Yet, the resulting space anisotropy (a distinctive feature of bone tissue, for instance assessed as *DA*) of HFMBs resembles that of natural bone more closely than the synthetic scaffold. The pore distribution in HD-CW HFMBs appears

also more regular than in the synthetic scaffold, less so in HD-LB HFMBs (as shown in the 3D rendering reported in Figures 6a-b and more extensively in the Supplemental material). In Table 1, the parameters of the space architecture of HD-HFMBs are compared to the natural and synthetic benchmarks. They show that the intermembrane space distribution in HD-CW HFMBs exhibits a mean pore size meeting the requirement of 300 μm for large pores to permit unhindered cell migration [22] and bears a rather good functional similarity to the benchmarks used. In fact, porosity, pore interconnectivity, mean pore size, and specific surface area are close to the natural tissue and the synthetic bone substitute. The connectivity density and degree of anisotropy are even more similar to the natural tissue than the commercial synthetic bone substitute. Such similarities suggest that engineering bone tissue in a HD-CW HFMB might facilitate cells access through the pore network in the ECS and their organization in an anisotropic tissue substitute resembling the bone better than some commercial scaffolds [44]. The similarity to natural bone tissue is particularly noteworthy in consideration of the large variability of bone trabecular tissue characteristics with the species and the site of harvesting.

4. Conclusions and future outlooks

Porosity, pore size distribution, pore interconnectivity and anisotropy, and pore specific surface area are known to affect cell migration, adhesion, differentiation, and nutrient supply in porous scaffolds for tissue engineering, and ultimately cell response and new tissue ingrowth. When hollow fiber membrane bioreactors are used for growing mammalian cells for healing or regenerating human tissues and organs, the importance of providing spaces and scaffolding surfaces in the bioreactor shell fostering cell organization and differentiation as in natural tissues is seldomly accounted for in their design. It is generally accepted that membrane distribution in the bioreactor shell is non-uniform and only partly within control of the designer.

In this study, we investigated whether and how it is possible to manufacture HFMBs with a controlled distribution of intermembrane spaces in the ECS and to challenge the assumption that

membrane distribution in HFMBs is intrinsically non-uniform and limits their use for medical applications. To this purpose, non-destructive microcomputed tomography (μCT) and image analysis techniques were effectively used to characterize the distribution of spaces and scaffolding surfaces in the shell of HFMBs varying in membrane packing density and bundling technique. Taken altogether the results that were obtained suggest that if hollow fiber membranes bundled in rolled cross-woven mats are arranged at high packing density in a HFMB the resulting shell space distribution may be engineered to be uniform, to exhibit a size distribution favoring cell migration and nutrient supply through the membrane bundle space, and to mimic the ECM structure of natural bone tissue, at least as well as some current commercial bone substitutes.

Efforts are under way to use μCT in time-lapse culture studies to investigate the actual evolution of stem cell growth, distribution and differentiation in the extracapillary space of clinically relevant HFMBs equipped with cross-wound mats of densely packed medical membranes and to compare it to those in commercial tissue engineering scaffolds.

CRediT authorship contribution statement

Giuseppe Falvo D'Urso Labate: Data curation, Formal analysis, Investigation, Writing - original draft. **Thomas De Schryver:** Investigation, Writing - review & editing. **Francesco Baino:** Investigation, Writing - review & editing. **Charlotte Debbaut:** Data curation, Formal analysis, Writing - original draft. **Gionata Fragomeni:** Data curation, Investigation, Writing - original draft.

Chiara Vitale-Brovarone: Methodology, Resources, Writing - review & editing. **Luc Van Hoorebeke:** Methodology, Resources, Supervision, Writing - review & editing. **Patrick Segers:** Funding acquisition, Supervision, Writing - review & editing. **Matthieu Boone:** Methodology, Resources, Supervision, Writing - review & editing. **Gerardo Catapano:** Conceptualization, Funding acquisition, Supervision, Writing - review & editing.

Declaration of competing interest

The authors declare that they have no known competing financial interests or personal relationships that could have appeared to influence the work reported in this paper.

References

[1] R.A. Knazek, P.M. Gullino, P.O. Kohler, R.L. Dedrick, Cell culture on artificial capillaries: an approach to tissue growth in vitro, Science 178 (1972) 65-67.

[2] G. Catapano, P. Czermak, R. Eibl, D. Eibl, R. Pörtner, Bioreactor Design and Scale-Up, in: R. Eibl, D. Eibl, R. Pörtner, G. Catapano, P. Czermak (Eds.), Cell and Tissue Reaction Engineering, Springer-Verlag, Berlin Heidelberg, 217-241 (2009).

[3] N. Wung, Acott S.M., Tosh D., Ellis MJ, Hollow Fibre Membrane Bioreactors for Tissue Engineering Applications, Biotechnol. Lett. 36(12) (2014 2357-2366. doi: 10.1007/s10529-014-1619-x.

[4] T.J. Chresand, D.J. Gillies, B.E. Dale, Optimum fiber spacing in a hollow fiber bioreactor, Biotechnol. Bioeng. 32 (1988) 983-992.

[5] H. Ye, D.B. Das, J. Triffit, Z.F. Cui, Modelling nutrient transport in hollow fibre membrane bioreactors for growing three-dimensional bone tissue, J. Membr. Sci. 272 (2006) 169–178.

[6] A.J. Davidson, M.J. Ellis, J.B. Chaudhuri, A theoretical method to improve and optimize the design of bioartificial livers, Biotechnol. Bioeng. 106(6) (2010) 980-988.

[7] L.J. Kelsey, M.R. Pillarella, A.L. Zydney, Theoretical analysis of convective flow profiles in a hollow-fiber membrane bioreactor, Chem. Eng. Sci. 45 (11) (1990) 3211–3220.

[8] J.D. Brotherton, P.C. Chau, Modeling of axial-Flow hollow fibre cell culture bioreactors, Biotechnol. Prog. 12 (1996) 575–590.

[9] J. Koska, B.D. Bowen, J.M.Piret, Protein transport in packed-bed ultrafiltration hollow-fibre bioreactors, Chem. Eng. Sci. 52(14) (1997) 2251-2263.

[10] I.E. De Napoli, E.M. Zanetti, G. Fragomeni, E. Giuzio, A.L. Audenino, G. Catapano, Transport modeling of convection-enhanced hollow fiber membrane bioreactors for therapeutic applications, J. Membrane Sci. 471 (2014) 347-361.

[11] G. Catapano, Bioreactors for bioartificial organs, in: R. Eibl, D. Eibl, R. Pörtner, G. Catapano, P. Czermak (Eds.), Cell and Tissue Reaction Engineering, Springer-Verlag, Berlin Heidelberg, 279-314 (2009).

[12] D.W. Scharp, Swanson C.J., Olack B.J., Latta P.P., Hegre O.D., Doherty E.J., Gentile F.T., Flavin K.S., Ansara M.F., Lacy P.E., Protection of Encapsulated Human Islets Implanted Without Immunosuppression in Patients With Type I or Type II Diabetes and in Nondiabetic Control Subjects, Diabetes 43(9) (1994) 1167-70. Doi: 10.2337/diab.43.9.1167.

[13] J.C. Gerlach, K. Zeilinger, J.F. Patzer II, Bioartificial liver systems: why, what, whither?, Regen. Med. 3(4) (2008) 575-95. doi: 10.2217/17460751.3.4.575.

[14] I.E. De Napoli, S. Scaglione, P. Giannoni, R. Quarto, G. Catapano, Mesenchymal stem cell culture in convection-enhanced hollow fibre membrane bioreactors for bone tissue engineering, J. Membrane Sci. 379 (2011) 341-352.

[15] S.P.S. Monga, M.S. Hout, M.J. Baun, A. Micsenyi, P. Muller, L. Tummalapalli, A.R. Ranade, J.-H. Luo, S.C. Strom, J.C. Gerlach, Mouse fetal liver cells in artificial capillary beds in three-dimensional four-compartment bioreactors, Am. J. Pathology 167(5) (2005) 1279-1292.

[16] S.N. Bhatia, G.H. Underhill, K.S. Zaret, I.J. Fox, 2014. Cell and tissue engineering for liver disease. Sci. Transl. Med. 2014 6(245), 245sr2, https://doi: 10.1126/scitranslmed.3005975.

[17] C. Pekor, J.C. Gerlach, I. Nettleship, E. Schmelzer, Induction of Hepatic and Endothelial Differentiation by Perfusion in a Three-Dimensional Cell Culture Model of Human Fetal Liver, Tissue Eng. Part C Methods, 21(7) (2015) 705–715. Doi: 10.1089/ten.tec.2014.0453

[18] G. Catapano, J.F. Patzer II, J.C. Gerlach, Transport advances in disposable bioreactors for liver tissue engineering, in: R. Eibl & D. Eibl (Eds.), Disposable Bioreactors, series "Advances in biochemical engineering / biotechnology", Vol. 115 Springer Verlag, Berlin and Heidelberg, 117-143 (2010). Doi: 10.1007/10_2008_34.

[19] A. Khademhosseini, R. Langer, A decade of progress in tissue engineering, Nature Protocols, 11(10) (2016) 1775-1781. Doi:10.1038/nprot.2016.123.

[20] P. Chan, K. W. Leong, Scaffolding in tissue engineering: general approaches and tissue-specific considerations, Eur. Spine J., 17(Suppl. 4) (2008) S467–S479. Doi 10.1007/s00586-008-0745-3.

[21] M.A. Fernandez-Yague, S.A. Abbah, L. McNamara, D.I. Zeugolis, A. Pandit, M.J. Biggs, Biomimetic approaches in bone tissue engineering: Integrating biological and physicomechanical strategies, Adv. Drug Deliv. Rev. 84 (2015) 1-29. https://doi: 10.1016/j.addr.2014.09.005.

[22] V. Karageorgiu, D. Kaplan, Porosity of 3D biomaterial scaffolds and osteogenesis, Biomaterials 26 (2005) 5474-5491.

[23] I. Noda, D.G. Brown-West, C.C. Gryte, Effect of flow maldistribution on hollow fiber dialysis - experimental studies, J. Membrane Sci. 5 (1979) 209-225.

[24] C. Ronco, A. Brendolani, C. Crepaldi, M. Rodighiero, P. Everard, M. Ballestri, G. Cappelli, M. Spittle, G. La Greca, Dialysate flow distribution in hollow fiber hemodialyzers with different dialysate pathway configurations, Int. J. Artif. Organs, 23(9) (2000) 601-609.

[25] C. Ronco, A. Brendolan, C. Crepaldi, M. Rodighiero, M. Scabardi, Blood and dialysate flow distributions in hollow-fiber hemodialyzers analyzed by computerized helical scanning technique, J. Am. Soc. Nephrol., 13(Suppl 1) (2002) S53-S61.

[26] J.C. Kim, J.H. Kim, H.-C. Kim, E. Kang, K.G. Kim, H.C. Kim, B.G. Min, C. Ronco, Effect of fiber structure on dialysate flow profile and hollow-fiber hemodialyzer reliability: CT perfusion study, Int. J. Artif. Organs, 31(11) (2008) 944-950.

[27] X. Yang, R. Wang, A.G. Fane, C.Y. Tang, I.G. Wenten, Membrane module design and dynamic shear-induced techniques to enhance liquid separation by hollow fiber modules: a review, Desalination and Water Treat., 51(16-18) (2013) 3604-3627.

[28] X. Yang, E.O. Fridjonsson, M.L. Johns, R. Wang, A.G. Fane, A non-invasive study of flow dynamics in membrane distillation hollow fiber modules using low-field nuclear magnetic resonance imaging (MRI), J. Membrane Sci., 451 (2014) 46–54.

[29] C.K. Poh, P.A. Hardy, Z. Liao, Z. Huang, W.R. Clark, D. Gao, Effect of flow baffles on the dialysate flow distribution of hollow-fiber hemodialyzers: a nonintrusive experimental study using MRI, J. Biomech. Eng., 125(4) (2003) 481-489. https://doi: 10.1115/1.1590355.

[30] J.P. Bhimani, R. Ouseph, R.A. Ward, Effect of increasing dialysate flow rate on diffusive mass transfer of urea, phosphate and β2-microglobulin during clinical haemodialysis, Nephrol. Dial. Transplant., 25 (2010) 3990–3995.

[31] G. Falvo D'Urso Labate, F. Baino, M. Terzini, A.L. Audenino, C. Vitale-Brovarone, P. Segers, R. Quarto, G. Catapano, Bone structural similarity score: a multiparametric tool to match properties of biomimetic bone substitutes with their target tissues, J. Appl. Biomater. Funct. Mater. 14(3) (2016) e277-e289.

[32] B. Masschaele, M. Dierick, D. Van Loo, M.N. Boone, L. Brabant, E. Pauwels, V. Cnudde, L. Van Hoorebeke, HECTOR: A 240kV micro-CT setup optimized for research, J Physics: Conf. Ser. 463 (2013) 012012. https://doi:10.1088/1742-6596/463/1/012012.

[33] S. Basu, Y. Bresler, O(N2 log2 N) filtered backprojection reconstruction algorithm for tomography. IEEE Trans. Image Proc. 9(10) (2010) 1760-73. https://doi: 10.1109/83.869187.

[34] A. Nafei, C.C. Danielsen, F. Linde, I. Hvid, Properties of growing trabecular ovine bone - Part I: Mechanical and physical properties, J. Bone Joint Surg. 82B (2000) 910-920.

[35] A. Odgaard, Quantification of cancellous bone architecture, in: S.C. Cowin (Ed.), Bone Mechanics Handbook, CRC Press, 2nd ed. Boca Raton, 2001, pp. 14.1-14.9.

[36] C. Sandino, P. Koliczek, D.D. McErlain, S.K. Boyd, Predicting the permeability of trabecular bone by micro-computed tomography and finite element modeling, J. Biomech. 47 (2014) 3129-3134.

[37] C. Igathinathane, L.O. Pordesimo, E.P. Columbus, W.D. Batchelor, S.R. Methuku, Shape identification and particles size distribution from basic shape parameters using ImageJ, Computers and Electronics in Agriculture, 63(2) (2008) 168-182. https://doi:10.1016/j.compag.2008.02.007

[38] M.J. Moore, E. Jabbari, E.L. Ritman, L. Lu, B.L. Currier, A.J. Windebank, M.J. Yaszemski, Quantitative analysis of interconnectivity of porous biodegradable scaffolds with micro-computed tomography, J. Biomed. Mater. Res. A 71(2) (2004) 258-267.

[39] Bruker microCT. CT-Analyser version 1.13 - The user's guide. 2013.

[40] M. Kiderlen, Estimating the Euler Characteristic of a planar set from a digital image, J. Vis. Commun. Image R. 17 (2006) 1237–1255.

[41] N.M. Razali, Y.B. Wah, Power comparison of Shapiro-Wilk, Kolmogorov-Smirnov, Lilliefors and Anderson-Darling tests, JOSMA 2(1) (2011) 21-33.

[42] U. Baurmeister, 1992. Woven hollow fiber double weft tape with knitted selvedge, US Patent 5,141,031 Akzo N.V. The Netherlands.

[43] G. Catapano, A. Wodetzki, U. Baurmeister, Blood flow outside regularly spaced hollow fibers: the future concept of membrane devices?, Int. J. Artif. Organs 15(4) (1992) 327-330.

[44] M.I. Gariboldi, S.M. Best, Effect of ceramic scaffold architectural parameters on biological response, Front. Bioeng. Biotechnol. 3 (2015) 151. doi: 10.3389/fbioe.2015.00151

	HD-LB HFMB	HD-CW HFMB	Natural EFT[*]	Synthetic NPHA scaffold[*]
Porosity, %	48.4±0.06	45.8±0.01	65.4±0.38	73.0±0.35
Pore interconnectivity, %	81	99	100	100
Mean pore size, mm	661±314	303±4	433±194	416±211
Specific surface area, mm^{-1}	4.03±0.35	5.71±0.05	8.05±0.67	9.38±0.09
Degree of anisotropy, -	0.90	0.97	0.72	0.08
Connectivity density, mm^{-3}	5.93±0.26	8.47±0.04	18.3±10.7	96.5±3.43

Table 1. Architectural parameters of the space distribution in HFMBs varying for membrane packing density and bundling technique: HD-LB HFMB - HFMBs prepared with loose bundles of membranes at high packing density; HD-CW HFMB - HFMBs prepared with rolled cross-woven mats of membranes at high packing density; Natural EFT – natural trabecular bone of equine femur; Scaffold NPHA – commercial narrow pore hydroxyapatite bone substitute. [*] data from [31].

Figure captions

Figure 1. Membrane bundling techniques used for this study: a) membranes arranged in loose bundle, LB; b) membranes arranged in cross-woven mats, CW. Figures reproduced with permission from the Separation and Purification Sciences Division (SPSD) of 3M, Wuppertal, Germany.

Figure 2. 3D bioreactor rendering. Scheme of the procedure to render in 3D the membranes (and space) distribution in the shell of hollow fiber membrane bioreactors in the shell-and-tube configuration starting from raw 2D images of bioreactor cross-sections acquired by micro-computed tomography: ECS – extracapillary space; ICS – intracapillary space; VOI – volume of interest.

Figure 3. Exemplary 2D images acquired by μCT of cross-sections of HFMBs equipped with low packing density of membranes provided in loose bundles (LD-LB HFMB). Images acquired at one end (a) or at the half-length (b) of the bioreactor.

Figure 4. Exemplary 2D images acquired by μCT of HFMB cross-sections. Images acquired at one end (a,b) or at the half-length (c-f) of HFMBs equipped with high packing density of membranes in various bundle types: a,c,e) loose bundles (HD-LB); b,d,f) cross-woven mats (HD-CW). Images in Figures 4e,f are magnifications of the images reported in Figures 4c,d, respectively.

Figure 5. Mean intermembrane porosity in various quadrants of bioreactor shell cross-sections. Images acquired at the half-length of HFMBs prepared with membranes differently bundled and packed at high membrane density: a) loose bundle, HD-LB; b) cross-wound mat, HD-CW. ROI-1 (solid lines) and ROI-2 (dashed line) identify a central or a peripheral zone in the HFMB cross-section, respectively, as shown in the inset of the left panel. In the same inset it is shown the quadrant (Q_i) position.

Figure 6. 3D rendering of micro-computed tomographic images of various scaffolding structures suitable for bone tissue engineering: a) HD-LB HFMB; b) HD-CW HFMB; c) trabecular bone of

natural equine femur, EFT [31]; d) commercial narrow-pore hydroxyapatite bone substitute, NPHA

[31]. Figures 6c,d reproduced with permission from SAGE Publishing Inc..